PROCEEDINGS, 41st Workshop on Geothermal Reservoir Engineering
Stanford University, Stanford, California, February 22-24, 2016
SGP-TR-209

Field Management and Expansion Potential of the Momotombo Geothermal Field Using Numerical Simulation and Conceptual Modeling

Dennis Kaspereit[1], William Rickard[1], William L. Osborn[1], Mary Mann[1] and Magdalena Perez[2]

[1] Geothermal Resource Group, 77530 Enfield Lane, Bldg. E, Palm Desert, CA 92211

[2] Momotombo Power Company, Reparto Las Cumbres, Casa D13, Managua, Nicaragua

dkaspereit@geothermalresourcegroup.com mperez@mpc.com.ni

Keywords: numerical simulation, conceptual model, expansion, field management, productivity index, cross-flow, optimization

ABSTRACT

The Momotombo geothermal field has been in development since the 1960s, with most drilling completed in the 1970s, and was on line with its first 35 MW_g geothermal flash power plant in September 1983. The field has had several operators in its 33-year operational history, with installed capacities of 35-77 MW_g and generation from 8-69 MW_e. Generation was 22.5 MW_e at the time of the study.

Momotombo Power Company recently became the owner/operator of the concession of the Momotombo field, and a complete assessment of wellfield performance and well conditions was initiated to assess the feasibility of increasing generation to 42 MW_g. This review included a numerical simulation of the field, which also requires a strong geologic conceptual model. Previous reservoir models focused on the producing field, but did not account for sources of pressure support to several wells from outside the core of the field area. A new conceptual model was developed, and a numerical simulation of the field was used to validate and adjust assumptions in the conceptual model, resulting in a very robust conceptual and numerical model.

The resulting, integrated model suggests the existence of an area of primary recharge and upwelling that is currently undeveloped and partially connected to the existing development, providing pressure and heat support to wells closest to that area. There appear to be significant developable reserves in this area, and additional exploration is recommended to determine the extent and possible secondary outflow areas.

Within the history matching process of the numerical model, two downhole well bore failures were identified. Candidates for well remediation have been identified to increase generation from existing wells to increase generation to 42 MW_e. Areas for expansion were revealed to better utilize installed capacity, and a plan to increase generation through the 15-year contract life will be implemented.

1. INTRODUCTION

The Momotombo geothermal field is located 40 km northwest of Managua, Nicaragua, on the northwestern shore of Lake Managua, at the foot of Volcan Momotombo, which forms part of the Cordillera de Los Marrabios, a chain of active volcanoes extending along the Nicaraguan Pacific coast (Figure 1). Since 1975, forty-seven wells have been drilled in the Momotombo field, ranging in depth from 310 m to 2839 m. Of these wells, 20 have been produced at some time, with 10 currently producing to the plant. Seven wells, mostly located in the eastern part of the wellfield, have been used for injection. Most injection was initiated in 2000, as the major portion of spent brine was previously disposed into Lake Managua.

Figure 1. Location of Momotombo geothermal field (after Martinez et al., 1988).

Momotombo Power Company (MPC) is the fifth operator, and currently has a 15-year concession to operate the field. The field was operated by Ormat from 1999 to 2013. The first 35 MW_g single flash geothermal plant at Momotombo was commissioned in September 1983, with a second 35 MW_g unit installed at the same site in 1989. A 7 MW_g binary bottoming cycle unit was installed in 2001, increasing the total installed capacity to 77 MW_g. Actual generation has been below installed capacity since 1986, ranging from a brief output of up to 69 MW_e in 1990, to a low of 8 MW_e in 1999 due to reservoir pressure decline, an influx of cooler meteoric water, and carbonate scale accumulation in production well bores. Ormat restored generation to a peak of 37 MW_e in 2002 after installation of the binary unit and well remediation, but output gradually declined to 22.5 MW_e at the time of this study.

MPC commissioned this study to explore the possibility of restoring generation to the 42 MW_g capacity of one flash plant and the binary unit. The goal of this study was to construct a numerical model to simulate the field history and current operational state, simulate forecasted generation cases to achieve the operational goal of 42 MW_g, and to provide an operational planning tool to investigate potential changes in the performance of specific wells and areas of the field. This is achieved by putting additional constraints on the model, including a significantly revised, detailed conceptual model that is consistent with the numerical simulation. Geology must be as much a part and focus of the process as the numerical simulation. The simulator can be used to test geologic assumptions and to build both the conceptual model and numerical simulation together to produce a robust, internally consistent model.

Some models, particularly those for financing, only seek to achieve a match in order to forecast the current configuration and future output, and can work well for this purpose, even with a limited number of constraints. If few constraints are used, there can be an infinite number of solutions that will produce a match, and modeling can become a glorified curve fitting with higher level exponents. These models tend to give erroneous forecasts if operating conditions are changed. For effective field management and near-term exploration, a model must be detailed and have sufficient constraints to make it a near-unique match. Additional data sets, such as fluid chemistry, reservoir tracer tests, or pressure transient tests are important, but the main requirement is a detailed conceptual model that is accurately represented in the numerical model structure. In reconciling the conceptual and numerical models for the developed field, as well as the surrounding undeveloped areas, the models become more refined in their geologic make up and reservoir properties. This can lead to expansion opportunities, identification of underperforming wells or wells requiring repair, wellfield optimization, and improved management of the resource.

2. CONCEPTUAL MODEL

2.1 Previous Model

The first step in a numerical simulation is to construct a geologic conceptual model to guide the physical structure of the numerical model. Figure 2 shows the conceptual model previously developed by others (Porras and Itoi, 2006 and Porras et al., 2007). This model assumed deep production and upflow in the western part of the field near the intersection of the southeast striking Momotombo fault and the northeast striking Bjornsson fault zone, into a shallow aquifer overriding a cold influx of water from the eastern side of the field. This model describes several important structures in the field, but is not sufficiently detailed to explain overall system recharge and injected fluid flow paths. It was also geologically inconsistent with the structural setting on the flank of an active volcano.

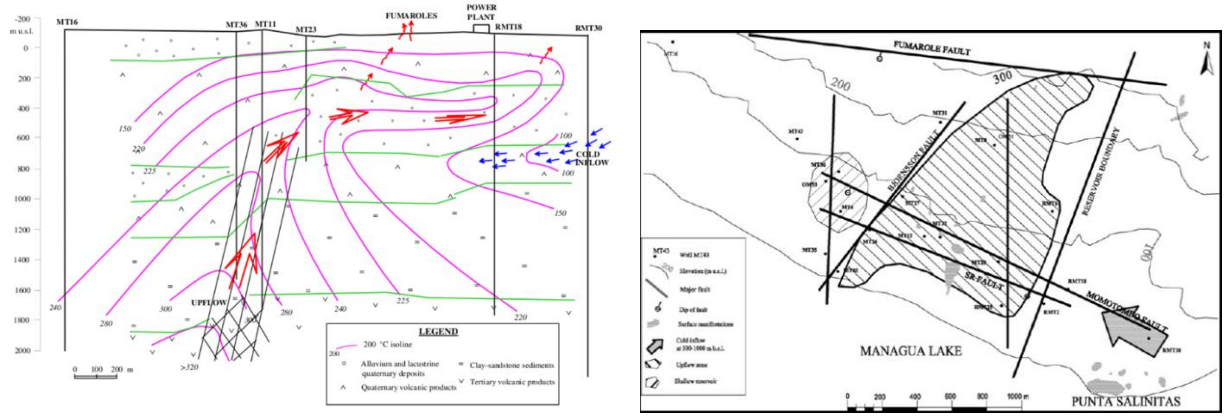

Figure 2. Previous conceptual model of the Momotombo geothermal field, with NW-SE cross section (left; Porras and Itori, 2006) along the Momotombo fault showing hot upflow from deep under the western part of the field, upflowing at the intersection with the Bjornsson fault zone, and cold inflow from the eastern part of the field, and plan view (right; Porras et al., 2007) showing locations of major faults, upflow zone and the shallow geothermal reservoir. Large grey arrow indicates the direction of cool water recharge.

2.2 Current Model

We have constructed a significantly revised conceptual model, with a structural setting consistent with volcanically-hosted geothermal systems. We propose that Momotombo possesses many of the characteristics of a typical volcanic-hosted geothermal system (Figure 3), where hot geothermal fluids ascend around the volcanic intrusion and then migrate, due to hydraulic gradient, downward and laterally through permeable formations on the flanks of the volcano. Fumaroles and the highest measured temperatures occur at higher elevations on the flank, and cooler fluid temperatures and chloride-rich springs occur at the foot of the volcano.

The revised conceptual model of the Momotombo geothermal system assumes that recharge originates beneath the steaming ground mapped at an elevation of about 500 m, and the hydraulic gradient transports fluids to the current field. The flow is southwest and south-southwest along the Perez and Bjornsson faults, respectively, and to the southeast under the Guatusa Plateau (Figure 4).

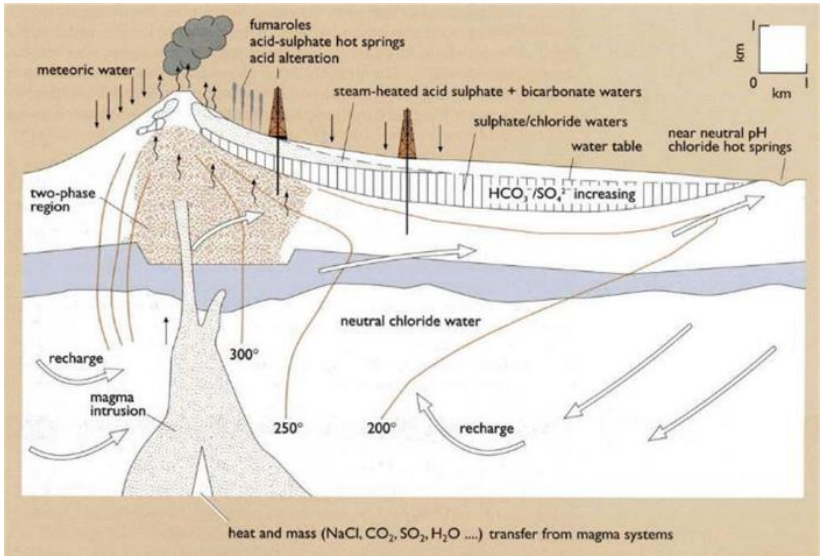

Figure 3. Conceptual model of a typical volcanically-hosted geothermal system, in which meteoric water percolates deep into the volcanic superstructure where it is heated by a body of magma. The hot fluid rises and boils to form steam, producing a two-phase zone and fumaroles at high elevation. The hydraulic gradient causes the residual liquid to migrate through permeable structures down the flank of the volcano where it can be accessed by drilling (note rig symbols at surface). Neutral pH chloride springs are distal from the volcano at outflow areas. Reproduced from Henley and Ellis (1983).

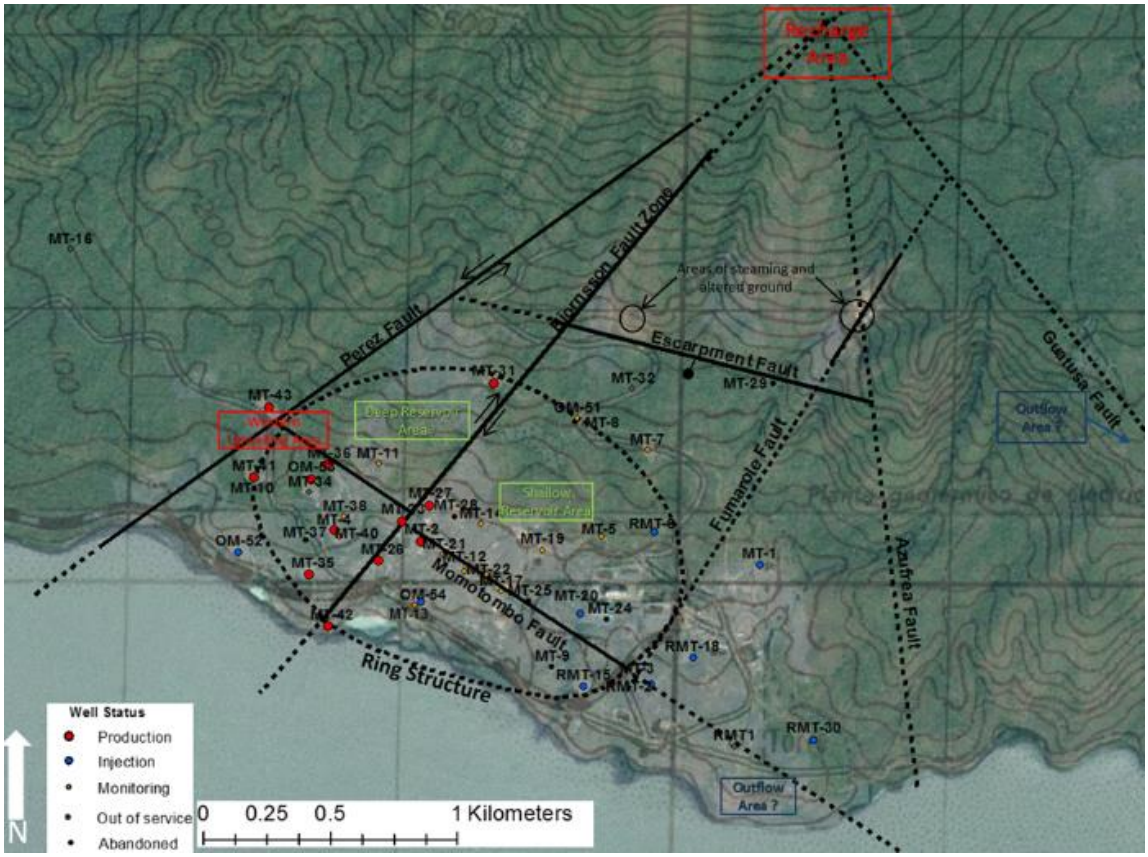

Figure 4. Momotombo wellfield map showing wellhead locations, postulated faults, and likely zones of recharge, upwelling and outflow, the suspected ring structure and other indicative thermal features in the new conceptual model.

2.3 Supporting Observations

A hydraulic gradient extends from the recharge area in northeast to the main production area in the southwest, and the northern fumaroles are hotter, with higher H_2S and more H_2 relative to CO_2 than fluids sampled in the south. These physical and chemical differences support the concept that the fumarole area overlies the recharge area for the Momotombo reservoir. From this primary upwelling, vapor separation occurs to feed the steaming ground above, and the boiled liquid, with elevated chloride concentration due to evaporation (Thermochem, 2008), flows southwest along the Perez fault and upwells near MT-43. The primary upwelling also flows laterally along the Bjornsson fault, at depths of about 500 m to 2000 m, past MT-31 toward the central production area, with continued major flows also down the Bjornsson fault to the intersection with the Momotombo fault, and southeasterly along the ring structure from MT-31.

Further evidence that recharge originates in the fumarole area is revealed by an investigation of temporal changes in temperature and pressure recorded in static well surveys conducted over a period of 25 years. Pressure drawdown that occurred in the reservoir in the 1990s drew cooler meteoric water into the reservoir from the east, and hot recharge from the north. This is illustrated by the progressive migration of the 205°C isotherm from southeast to northwest as the cooler meteoric water breakthrough occurred (Figure 5, left). The isotherms are more closely spaced in the later years at the greatest depths. The upward migration of the isotherms as the cool water influx occurs suggests that a barrier exits at depth along this line.

The 1995 isotherm seems to bulge back toward the previous surface, indicating a localized resistance to the cold influx. In a plan view (Figure 5, right), it is apparent that the bulge is to the south, indicating that it is influenced strongly by hotter input from the north and northwest, coincident with the strike of the Bjornsson fault in the area where MT-31 is located. Also apparent in the isotherms surfaces is a retreat in the year-2000 surface along the Momotombo fault. This is due to a sharp pressure increase in the deep reservoir in 1997 that is discussed later in the MT-10 cross flow section. The top of the 2005 isotherm surface follows the Bjornsson fault. This is assumed to be caused by a drop in pressure in the deep reservoir from an event in 2001, also discussed later in the MT-10 cross flow section.

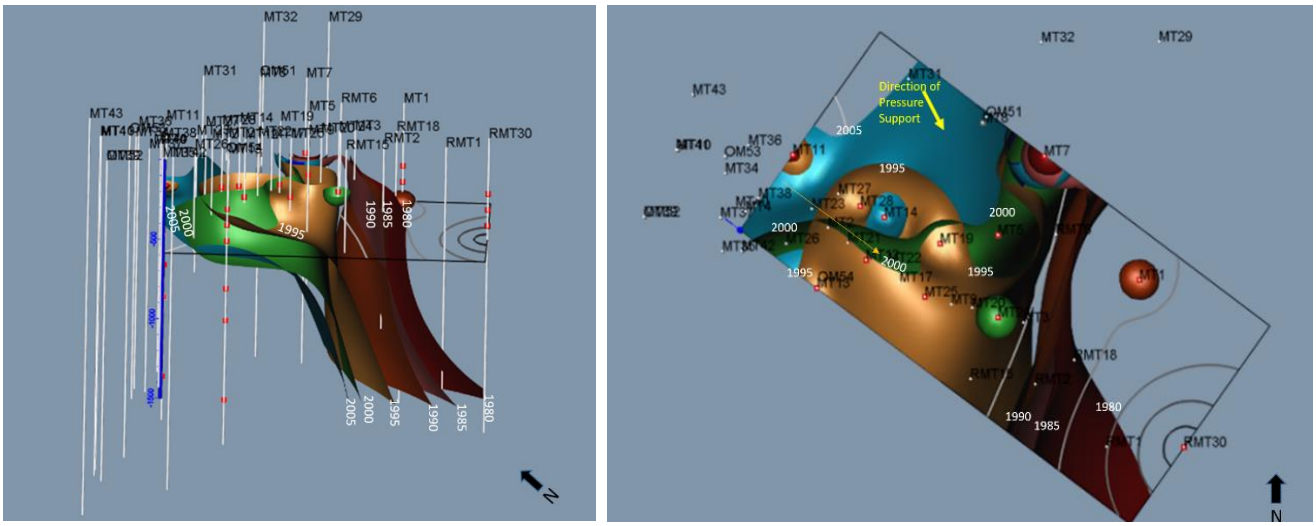

Figures 5. Cross-sectional view (left) to the northeast (model north), showing the 205°C isotherm migrating from southeast to northwest as an influx of cooler meteoric water occurred. Each 205°C isotherm surface represents a data set collected every five years, from the period 1980-2005. Plan view (right) of 205°C isotherms for 1980-2005 (every 5 years), showing localized resistance to northeast migration of cooler meteoric water influx, likely caused by hot fluid recharge from the area north of MT-31 (yellow arrow) in the 1995 surface, and resistance from Northwest along Momotombo fault in 2000 surface, most likely from a cross flow in MT-10.

Figure 6 is a NW-SE conceptual model cross section near and on strike with the Momotombo fault, showing the postulated flow paths through the reservoir in the native state and initial years of operation. After originating in the northern recharge area, fluid flows southwest along the Perez fault at great depth and into deep pay zones, southeast and upward into the Bjornsson fault, and then southeast in a shallow formation, predominately in the Momotombo fault and ring structure, overriding cooler meteoric water.

When the field was initially produced, the reservoir pressure declined sharply and there was a cold water influx toward the resulting low pressure sink. At present, the cold influx from the southeast seems to be in balance with the hot deeper reservoir. This ‘balance point’, where the influx from the southeast and flow from the deeper reservoir counteract each other, has been established as the pressure in the deeper reservoir has rebounded to near native-state levels (Figure 7).

Geophysical evidence corroborates upwelling along the Perez fault and lateral flow to the Bjornsson fault zone. Employing the findings of a report by Trans-Pacific Geothermal Corporation (2000), the aeromagnetic signature reveals the likely strike of faults in the Momotombo field. A northeast trending magnetic high on the west side of the field could be the signature of a dike swarm intruded

along a plane of weakness that reveals the strike of the Perez fault. Additional evidence, including mapping of seismic activity and lineament analysis, supports recharge from the north along northeast-trending faults.

We have used geophysics, particularly aeromagnetic data, to determine the likely strike of the Guatusa fault which, like the Momotombo fault to the south, may demonstrate significant permeability. We postulate that this fault allows outflow into a broad area to the southeast known as the Guatusa Plateau. The aerial extent of the Guatusa anomaly is difficult to assess due to a paucity of data. We only have the geophysical signature to use in the assessment. Calibration in the model consisted of tuning the permeability to produce backpressure to simulate the proper flow to the south to match the support seen from the north.

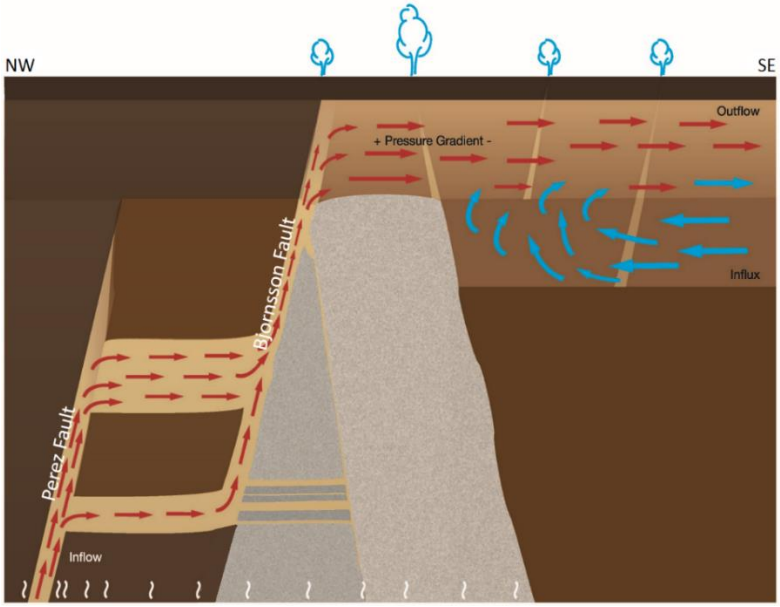

Figures 6. Conceptual model cross-section, from northwest to southeast along the Momotombo fault, showing postulated initial fluid flow patterns before cross-flow in MT-10. Fluid flows upward and laterally to the southeast from the western-most Perez fault, then upward through the intersection of the Momotombo and Bjornsson faults, continuing southeast along the Momotombo fault, overriding the cooler meteoric water migrating northwestward toward lower pressure.

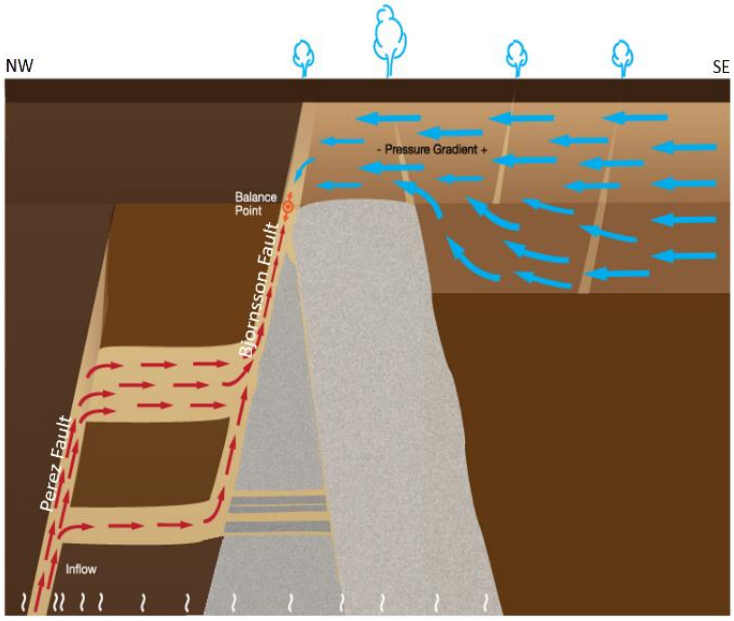

Figure 7. An underbalanced production reservoir causes a strong influx of cooler meteoric water to migrate northwestward until the cross-flow in MT-10 increased pressure in the deep producing reservoir, providing resistance to the influx of meteoric water and forming a balance point, stalling both flows at that balance point.

2.4 Ring Structure

A principal feature of the conceptual model is an apparent ring structure around the main wellfield. This structure, possibly a parasitic cone or remnant caldera now covered by subsequent eruptions, provides a plausible explanation for implied fault structures, the results of tracer studies conducted in 2001 and 2015, as well as observed pressure responses. Tracer injected into RMT-15 or MT-18 is first detected in MT-31, before breakthrough is observed along the Momotombo Fault in MT-2 and in the central production area around MT-27. This suggests that a northwest trending permeability conduit is present from RMT-15 to MT-31. The core of the apparent ring structure is dominated by a low permeability barrier, as portrayed in Figure 7, which is consistent with the presence of a volcanic neck.

3. MODEL STRUCTURE

This model was completed using TOUGH2 simulation code within a PetraSim environment. The model boundaries were selected to include all wells, with a surrounding buffer zone in all directions to eliminate boundary effects and encompass significant geographic and hydrologic features, including Volcan Momotombo and Lake Managua.

The model grid is orientated N30E, parallel to the axis of the Bjornsson fault and perpendicular to the Momotombo fault, which are major fluid conduits. Aligning the model with these features allows for finer gridding associated with these features. Both matrix and dual porosity parameters were investigated. Dual porosity was ineffective because the MINC method resulted in excessive homogenization of fracture permeability, and the Momotombo system appears to have a more discrete fracture distribution.

3.1 Dimensions

The aerial extent of the model is 8,800 meters by 5,400 meters (Figure 8). The model is divided into 15,080 grid blocks in a distribution of 40 blocks in the x–direction, 29 blocks in the y-direction, and 13 blocks in the z-direction. The origin is in the southwest corner at mean sea level. The vertical extent is 4257 meters, from 1,257 meters above mean sea level (masl) at the top of the Momotombo volcano, to a depth of -3,000 masl. Grid blocks vary in size from 25 meters by 50 meters along the Bjornsson fault within the producing area, to 2,000 meters by 2,000 meters at the corners.

Grid blocks in the northern area are intermediate in size, in part to not give a false sense of accuracy, as well as to speed up execution time of the simulation runs. Figure 9 shows the relative block sizes in the wellfield, the northern upflow area, and the model edges. It also shows the relative thickness of the different layers in relation to depth.

The conceptual model elements controlling fluid flow and temperature are accounted for in the model structure by assigning rock properties to different blocks that allow or impede flow in accordance to the role that the element plays in the conceptual model. The model uses 54 different rock materials in 13 layers.

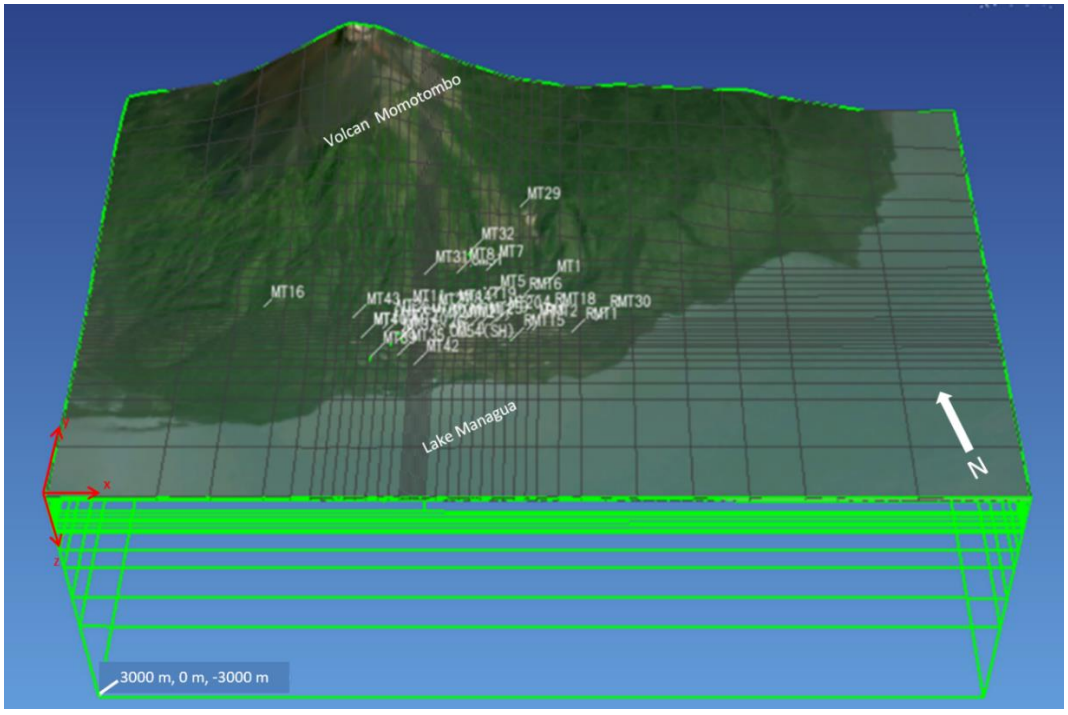

Figure 8. Model grid block and layer distribution, with y-axis oriented N30E, 8.8 Km northwest to southeast and 5.4 Km northeast to southwest, with base at elevation of -3 Km masl.

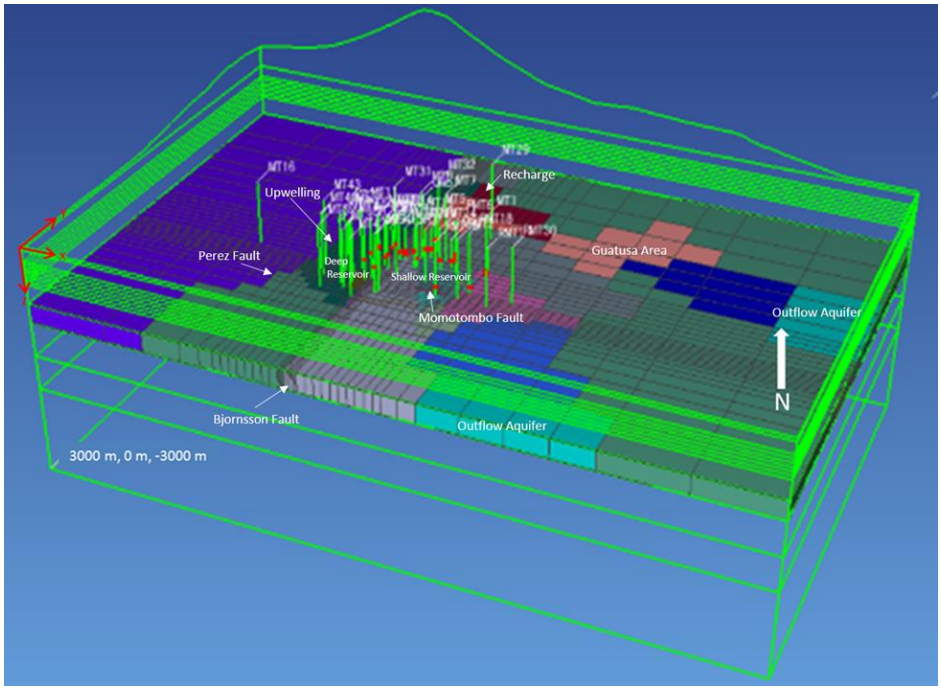

Figure 9. Block distribution, with colored blocks showing rock properties in -700 to -950 masl layer.

4. PRESSURE

In the early years of operation at Momotombo, produced fluids were not injected after heat extraction in the power plant. Instead, most of the heat-depleted fluids were disposed into the lake. This caused a large pressure drawdown in the reservoir and the formation of two-phase conditions in large areas of the reservoir. As production continued without reservoir injection, the reservoir vapor collapsed as shallow, cooler water encroached.

4.1 MT-11

MT-11 is the primary observation well for the deep reservoir, although it is shallow and the data must be corrected to correlate with the deep zone. A good pressure match with the model is shown in Figure 10. This detailed pressure observation data has been invaluable in deciphering the complex history of the surrounding reservoir, which is described below.

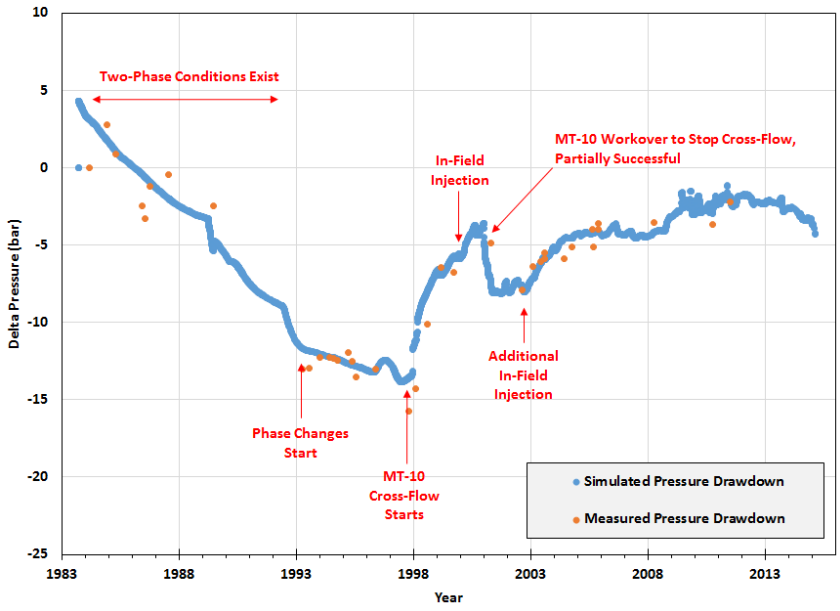

Figure 10. Pressure history match of observation well MT-11 with events affecting pressure response, including the assumed start of cross-flow in MT-10 in 1997 and the attempt to repair the cross-flow in 2001.

4.2 MT-10

In 1997, an event apparently occurred that introduced a large influx of water into the deeper reservoir. It is likely that this event was a shallow casing failure in MT-10 that allowed cross-flow from a shallow, cooler aquifer to a deeper, hotter zone in the well. This failure caused the deep reservoir pressure to increase rapidly, providing pressure support and resistance to the shallow meteoric water that was encroaching. This resistance can be seen in the evolution of shallow reservoir temperatures which created a pressure 'balance point' (Figure 7) in the Bjornsson fault where the impacts of shallow injection and cool water encroachment to the southeast are balanced by recharge and deep influx of hotter fluids from the northwest.

The pressure continued to rise, stabilizing slightly as conditions reached the original state pressure. In 2000, injection into the reservoir was initiated. In 2001, a workover to plug and abandon MT-10 was completed in an attempt to stop the cross-flow. However, it is apparent that this workover was only partially successful; reservoir pressure declined and stabilized, but above previous levels. With additional injection in 2002, there was a slow recovery of reservoir pressure.

To confirm that MT-10 was the cause of a dramatic change in reservoir pressure, we conducted two 'what-if' simulations to compare to the matched pressure history in observation well MT-11: (1) without the cross-flow in MT-10 and continued fluid disposal into the lake and, (2) without the cross-flow in MT-10 and injection into the reservoir (Figure 11).

Because well production and power generation reached a low of 8 MW_e in 1997, pressure decline in the next few years was relatively low due to the lack of mass withdrawal from the reservoir. Increased production after well workovers in the late 1990s would have resulted in a resumption of severe decline if cross-flow in MT-10 did not occur and fluid disposal into the lake continued. If, instead, the cross-flow had not happened but injection into the reservoir occurred, we would expect an increase in pressure from 2002, mirroring the history-matched rise and, therefore, that rise can be attributed to the injection relocation. Injection relocation alone, without the cross-flow in MT-10, would have taken until 2009 to surpass the 1997 pressure level and production would have been significantly lower. The injection relocation-only case does not match measured data; additional influx was needed to produce a match, and MT-10 was known to have a cross-flow with a very measured effect in MT-41. This confirms that despite the abandonment, there is continued downhole cross-flow in MT-10. If no cross-flow had occurred in MT-10 and there was no injection into the reservoir, pressure would have continued to decline and the reservoir would likely would not be producing today.

The influence of cross-flow in MT-10 shows a wide areal extent. However, because this outflow is relatively deep and below all of the other production wells in the field, and thus the positive effects of additional pressure support far outweigh any possible negative effects, such as thermal breakthrough. In its current configuration, the reservoir is not expected to experience pressure depletion, and should be sustainable at current levels in the future. However, temperature decline due to injection breakthrough is a major concern. Thermal breakthrough can be effectively managed using the numerical model as a planning tool and relocation of injection to optimum locations.

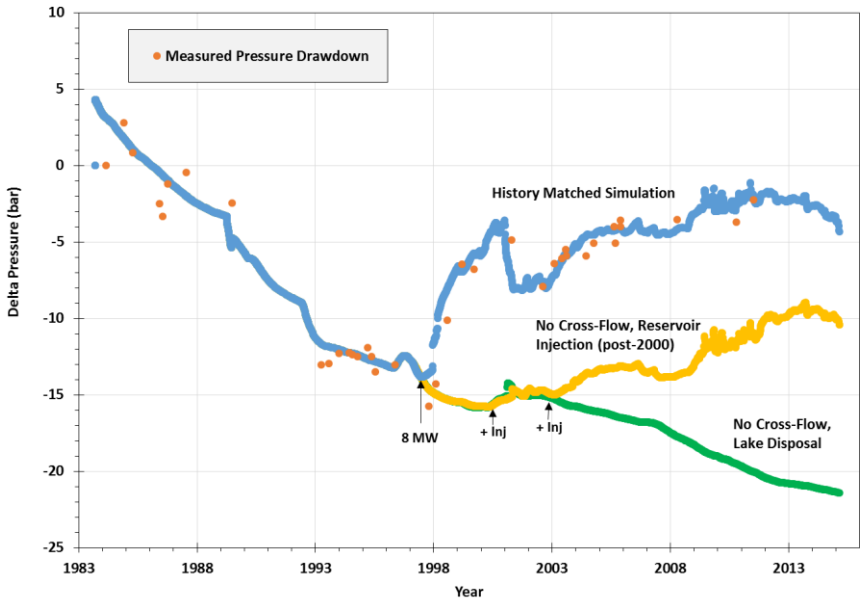

Figure 11. MT-11 pressure history match with three modeled cases, including the matched history and two 'what-if' scenarios. The matched history is shown by the blue curve, and reflects the actual history after an attempt to plug and abandon MT-10 in 2001 and the start of injection into the reservoir in 2000 and 2002. The green curve models no occurrence of a cross-flow in MT-10 and continued fluid disposal into Lake Managua. The yellow curve also models no cross-flow in MT-10, but with the injection into the reservoir added in 2000 and 2002 (red arrows).

4.3 MT-13

As stated previously, the influx of fluid in 1997 had to come from the deep reservoir and created a balance point at the top of the Bjornsson fault. Therefore, the response shown in Figure 12 requires that MT-13 be connected to the deeper reservoir on the opposite side of the fault. Lithological correlations also suggest that MT-13 is connected to the deeper western reservoir and to MT-11, possibly in a common fault block, which is supported by the pressure response.

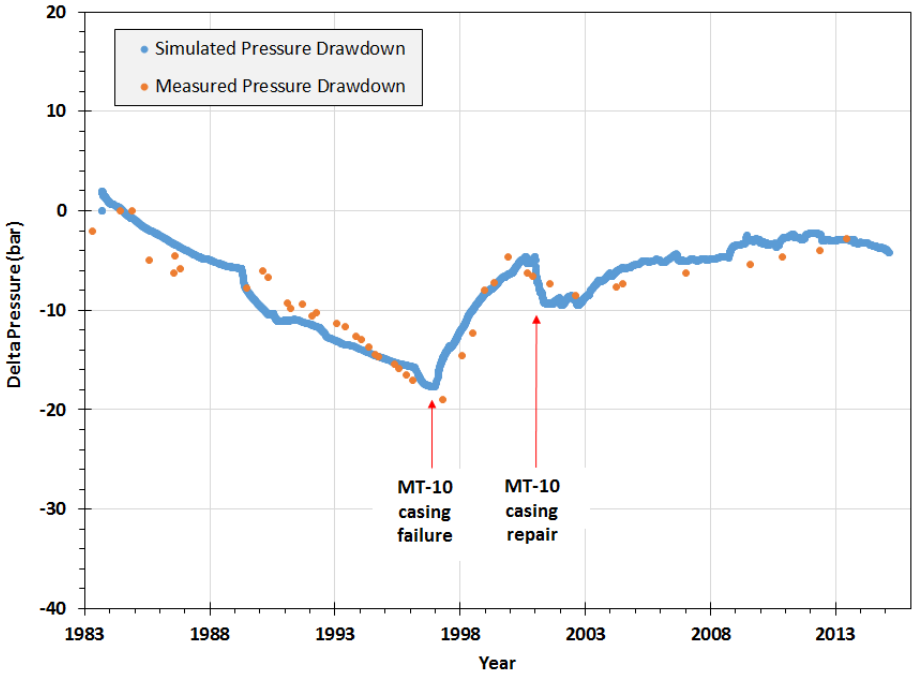

Figure 12. MT-13 pressure history match demonstrating connection to deep reservoir based on response to MT-10. The pressure surge observed in MT-13 due to a casing failure in MT-10 in 1997, and subsequent pressure decline after attempted repair in 2001, confirms that the deep zone in MT-13 is connected to the deep reservoir west of the Bjornsson fault.

5. CROSS-FLOW IN OM-54

Two wells, MT-23 (Figure 13) and MT-26, demonstrate production histories that suggest a cooling event and a sharp drop in enthalpy in 2002. These wells demonstrate anomalous low enthalpy (post-2002) relative to the surrounding reservoir. Several potential sources of cold water near these wells were investigated. A good match of actual versus modeled data was achieved with the introduction of shallow cold water sourced near MT-23 and MT-26. Additional simulations indicate that invasion of cool water (injection or meteoric) from the east side of the wellfield, or from MT-10, is not affecting these wells.

Casing leaks, wherein cooler water enters the well bore and mixes with the production flow, are a possibility, and simulating this provided an excellent match. Both wells were acidized in 2002, but it is not likely both would fail at the same time. Instead, we found excellent matches with a cold flow entering shallow into the Bjornsson fault between MT-23 and MT-26, and suspected that this shallow flow could be coming from OM-54.

OM-54 is an idle, directionally drilled well located 200-400 meters to the south of MT-23 and MT-26. OM-54 was drilled in mid-2002 on the same pad as MT-13, and at same time as the observed enthalpy decline. Drilling reports indicate cementing difficulties and a low flowing temperature during the OM-54 flow test. While simulating MT-10 pressures, it was determined that the deep part of the MT-13 area was in good hydraulic connection with the western deep field, so another rock type was added to the model structure west of a line extending from the ring structure passing near MT-13 and into the MT-23 and MT-26 area. Assuming that this structure is permeable and extends to shallow depths, and modifying block parameters accordingly, we achieved excellent history matches with MT-23 and MT-26.

Temperature surveys at 300 m in OM-54 that were conducted at the time of the initial flow test show an initial temperature increase to temperatures similar to MT-13 before the test, located on the same well pad, then a sharp drop during the test after heating up (Figure 14). Based on these observations, it appears that a bad cement job failed during the test and does not isolate the zones behind the casing. This allows cross-flow to occur in the annulus around the casing. Drilling records indicate that mud losses occurred at this depth, indicating permeability in an area of the field known to have permeability at this depth.

The temperature versus depth profile in OM-54 (Figure 15) shows an isothermal section from about 225 m to 450 m, indicative of flow behind casing. The MT-13 temperature profile shows that the original temperature was higher at 450 m than at 250 m, suggesting that

the annular cross flow in an upward direction from 450 m. The flow needed to match the anomalous low enthalpies in MT-23 and MT-26 is 33 kg/s. Thus, we conclude that the poorly cemented annular space in OM-54 is allowing flow upward flow from 450 m and exiting the annulus at about 225 m. This flow enters the Bjornsson fault, adversely affecting several nearby wells, including MT-23 and MT-26. Further confirmation of the annular void might be detected with an ultrasonic inspection tool (USIT), but a cement bond log would also be diagnostic. Eliminating the annular flow in OM-54 would require perforation and a cement squeeze, but the risk of an incomplete cement job is significant. The long-term effects of this shallow cool flow, and the potential benefits to correcting this problem will be discussed in a following section.

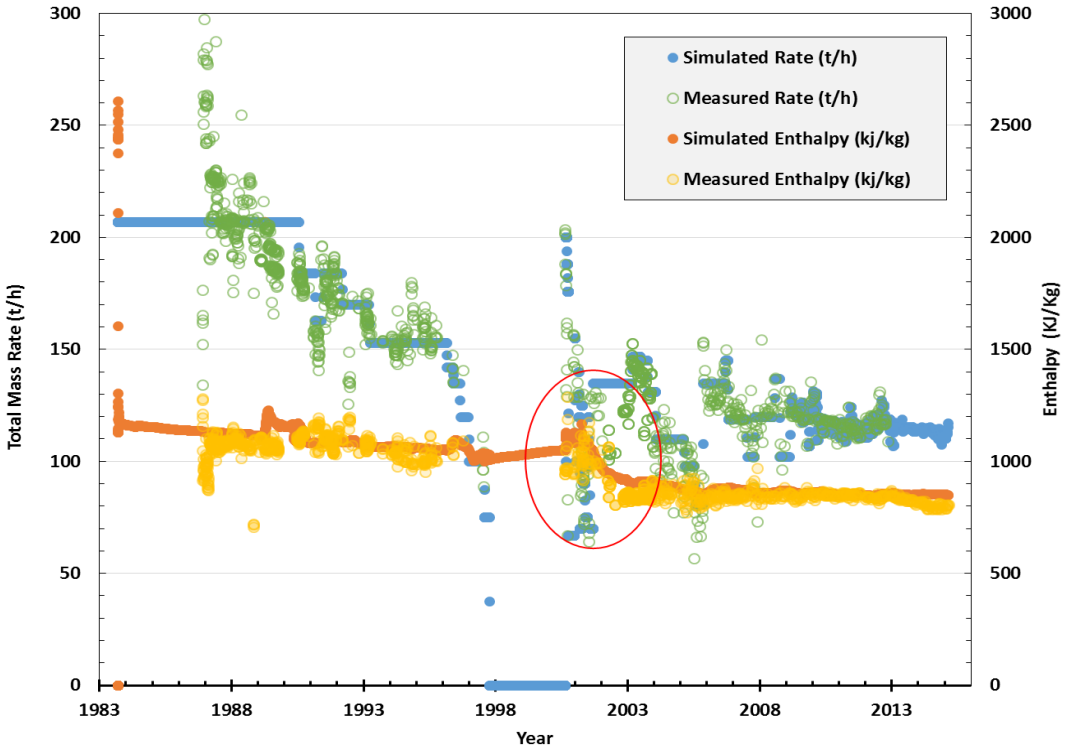

Figure 13. Enthalpy history match of MT-23. A sharp drop in measured enthalpy (red sphere) is coincident with the initial completion and testing of OM-54. A successful history match was achieved by simulating the addition of 33 Kg/s cool water flow into the Bjornsson fault at a shallow depth from a cross-flow in OM-54. MT-26 shows a similar enthalpy drop and successful match.

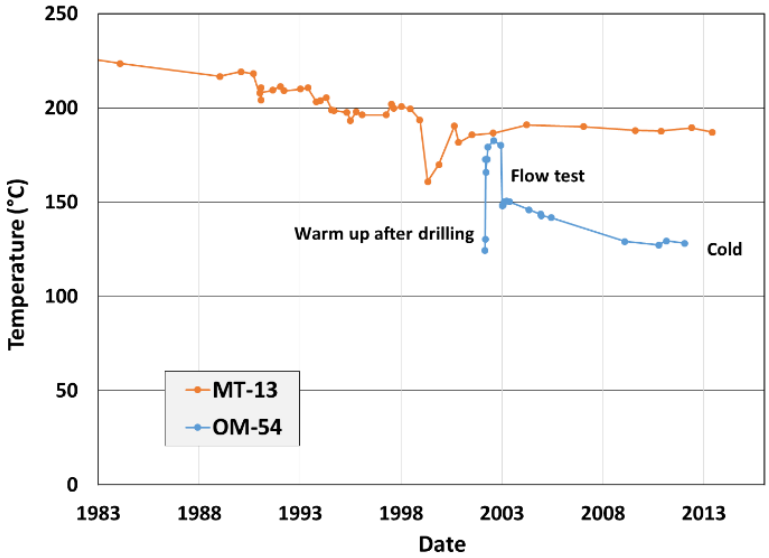

Figure 14. Temperature versus time at 300 m in OM-54 and MT-13, demonstrating an initial correlation between measured shallow temperatures in these adjacent wells, then a sharp drop in OM-54, presumed to be due to shallow casing damage at time of initial flow.

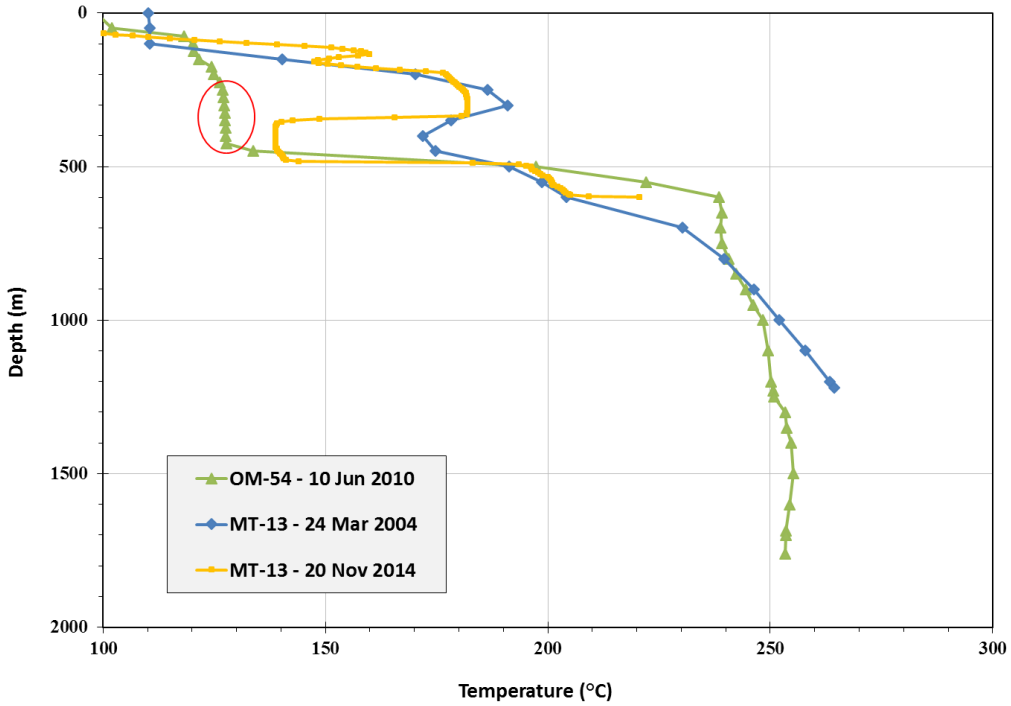

Figure 15. Static temperature profiles in OM-54 and MT-13, showing an isothermal section at 250-450 m (red circle) in OM 54 that is indicative of cross-flow. The shallower cooler section at 250-350 m is not present in MT-13, indicating upflow from the 350-450 m cool section in both wells.

6. PRODUCTIVITY STUDY

Production forecast simulations rely on the use of a productivity index (PI), and the differential pressure between the reservoir and wellbore, to calculate flow rate. In a history match, the production flow rate is a defined variable, and the reservoir response is calibrated to match that given production. Reversing the PI calculation used in the forecast, and applying it to a calibrated history match allows determination of the PI required to match the measured flow during the history matching period. The output is apparent PI versus time. If there is no damage, scale deposition, or well bore reconfiguration, this should produce a trend of zero slope in the PI vs time graph. Scale deposition is often evidenced by a declining PI, whereas a step change downward in PI may indicate well bore damage. Acid jobs or other workovers should produce an upward step in PI and can be used to assess the relative effectiveness compared to other potential remedial activities. This technique was used in this simulation study to assess the health of the existing wells. This general assessment of the well field was needed due to the long period of time since a workover program was conducted. Three examples are described below.

6.1 MT-27

MT-27 is an example of a healthy well that exhibits a constant PI for the last 15 years, and is not a candidate for an acid job (Figure 16). The acid job completed in 2006 showed no improvement, as would be expected from the flat PI prior to acidizing.

6.2 MT-26

MT-26 displays a steady decline in PI over the last 15 years (Figure 16). This well is impacted by OM-54 cross-flow, which could be exacerbating the scaling tendency in this well. MT-26 has the greatest potential for increased production from an acid job (aside from OM-53). A reformulated acid job is recommended. If successful, a similar acid job in MT-23 should be evaluated. Without a remedial job in OM-54 however, scaling in the well will most likely continue.

6.3 MT-31

MT-31, one of the most productive wells in the field, has demonstrated a relatively constant PI, except for an event in 2004-2005 that resulted in a very sharp decline that was probably caused by rapid calcium carbonate scale deposition (Figure 16). A successful acid job in 2006 restored production and probably increased generation about 3 MW_g. The PI then remained relatively steady until a decline began in 2008, possibly under-dosing of scale inhibitor chemical. An acid job in 2013 resulted in a minor increase in productivity of about 15 ton/hr, restoring flow to the pre-2008 level. However, this work was probably not cost effective, given the minor increase in production flow rate and resulting generation of less than 0.5 MW_g. This well history illustrates the effective use of acid to restore production from severe declines, but also shows the limitations of enhancing PI beyond previous highs.

The same technique was used on the injection wells. The apparent injectivity indices versus time for the injection wells shows over 50% of the initial injectivity has been, and continues to be, lost in the field. This makes the injection wells the best target for acid jobs to remove the effects of silica scale deposition occurring in the wells.

Unlike the late 1990s, when the effects of calcium carbonate scale deposition were very apparent, with flow loss due to pressure limited production, the current flow rate is more consistent and generation decline is mostly caused by thermal decay. Workovers and acid jobs alone will not restore Momotombo to 42 MW_g generation.

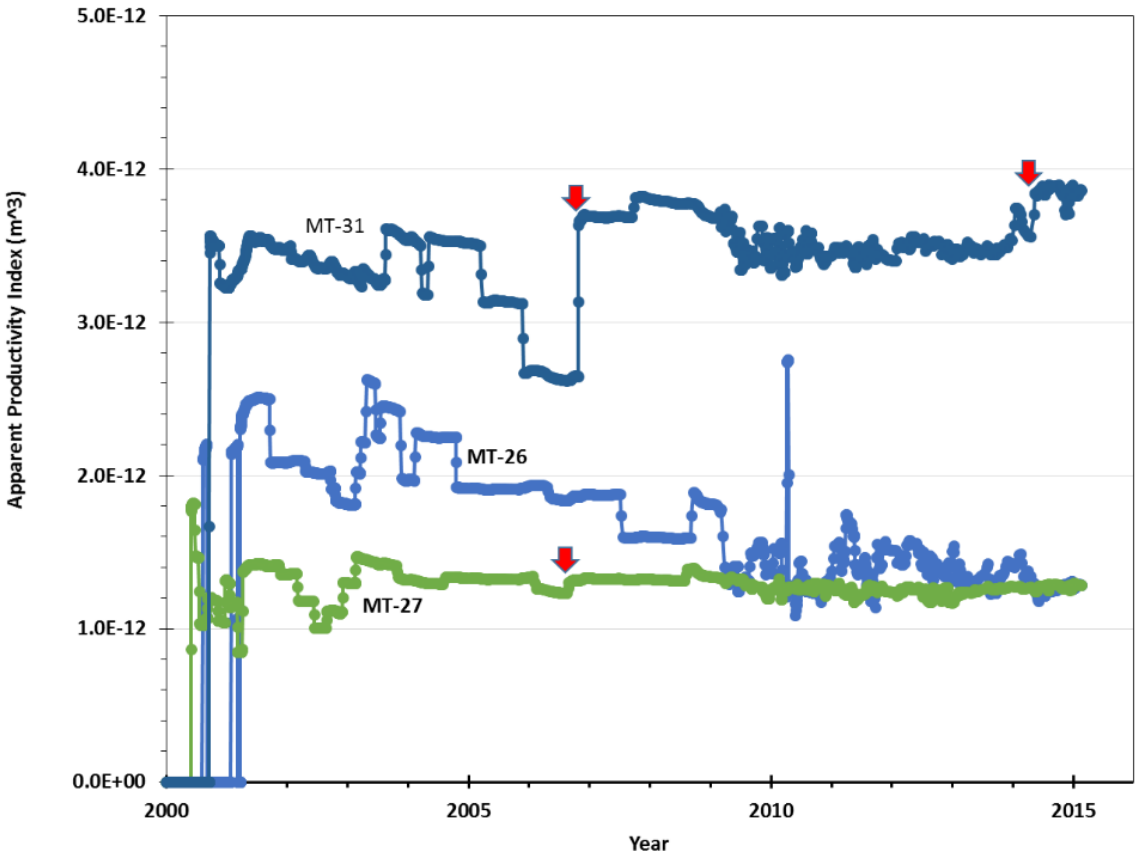

Figure 16. Three example Apparent Productivity Index curves. Red arrows indicated acid jobs.

7. INJECTION OPTIMIZATION

Numerous injection optimization cases were investigated, starting with individual wells. A summary of the major results are shown in Figure 17. The most striking feature is the thermal degradation indicated by the Base Case, in particular after 2020, with a decline to 14 MW_e by 2045. This degradation was noted by previous investigators and outfield injection (moving all injection outside the limits of the field) has been suggested to eliminate the thermal decline. Our simulations show that while the thermal degradation due to injection would stop, there would be a rapid loss of pressure support if all injection was moved outside of the current production area. Outfield injection is expected to result in a very significant early loss of generation, and is not considered a viable option. However, the outfield injection case provides a good indication of the decline curve slope without thermal decline from injection. From the graph it can be seen that the best injection scenarios minimize the thermal effects from injection while highlighting the thermal drop in the base case. After quickly minimizing the thermal decline, optimization became an exercise in finding the optimum pressure support with minimal thermal decay.

Two wells, RMT-15 and RMT-6, inject in shallower intervals within the ring structure and the high permeability that occurs in these zones. Moving the injection from these wells into wells or locations outside the ring structure eliminates most of the thermal decay related to injection, as shown by the brown curve in Figure 17.

Further optimization is obtained with strategic deep injection, mostly below the bottom producing zones in the deeper reservoir. This pressure support results in a steady increase in generation over the next three years to 23.5 MW_e, before returning to a decline slope just slightly less than that of just moving injection outside the ring structure, to an endpoint of 19 MW_e.

Fixing the cross-flow in OM-54, in addition to the injection optimization, provides an immediate boost and a three year increase to 25.5 MW_e, as compared to 23.5 MW_e from optimization alone. With the repair and optimization, the generation would stay above the current generation level past the end of the concession period, and even be at 21 MW_e at the end of the 30 year forecast period. The

long term slope is also better than the optimized case, but that is due to eliminating the thermal effects of the OM-54 cross-flow from spreading to additional wells and not injection related. The same boost and gain can also be applied on the outside the ring structure case without optimization (not shown) with a peak of 24 MW_e, an end of concession value of 22 MW_e, and an end of forecast value of 20.5 MW_e. Moving injection from RMT-6 and RMT-15 to outside the ring structure, and repairing OM-54 to stop cross-flow, are the quickest and least costly methods for minimizing thermal decline.

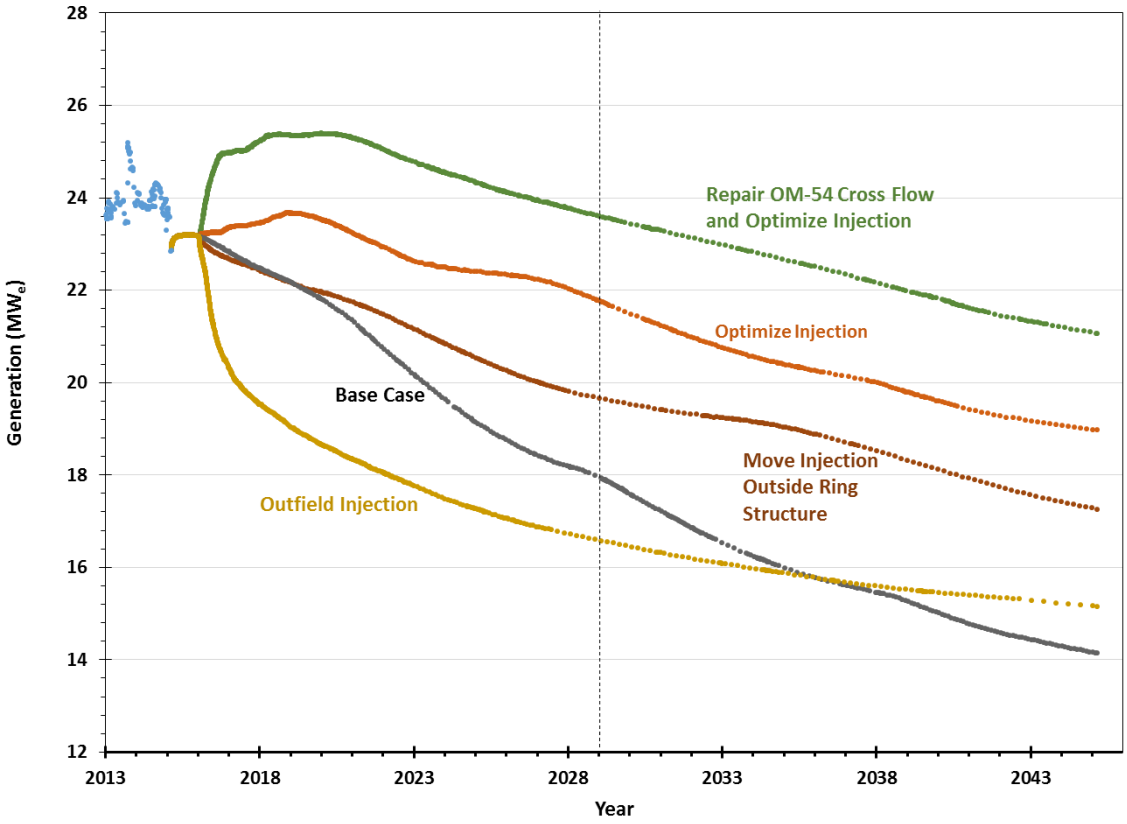

Figure 17. Summary of injection optimization. Shown for comparison is the current injection wellfield configuration (Base Case), injection relocated outside the ring structure and injection moved outside the reservoir (Outfield Injection). The optimized injection case, and optimized injection with the cross-flow in OM-54 repaired are also shown.

8. PRODUCTION OPTIMIZATION

8.1 Exiting Southern Area

To optimize the production wellfield, a series of potential drilling locations were identified. These included infield locations, locations in the northern zone of primary recharge, in the Guatusa area, in a secondary zone of postulated upwelling, and in the deep feeding fault to the west. Simulations of the performance of a production well completed at each location were added to the base case. Results varied, with initial increases in power generation of 2 MW_e to 6.5 MW_e depending on the well location. At the end of the concession period, the increase varies from 0.5 MW_e to 4.5 MW_e, and at the end of the forecast period from zero to 3.5 MW_e.

It appears that there are some deep targets in the current reservoir, and a medium depth target under MT-31. Viable shallow drilling targets within the currently developed wellfield have been exhausted. Infield drilling is limited to one, possibly two wells, in the northern part of the current deep reservoir.

A composite reservoir simulation (Figure 18) indicates that power generation at Momotombo can be increased significantly by completing remedial work on existing wells and drilling two new wells, and implementing injection optimization in the existing wellfield. These simulations include both the deleterious effects of mineral deposition in the wells, and periodic workovers or acid jobs to improve well performance. The target of 42 MW_g is approached, but simulation suggests that the existing southern area has the potential to generate only about 39 MW_e, declining to 32 MW_e at the end of the concession and to 27 MW_e at the end of the forecast period.

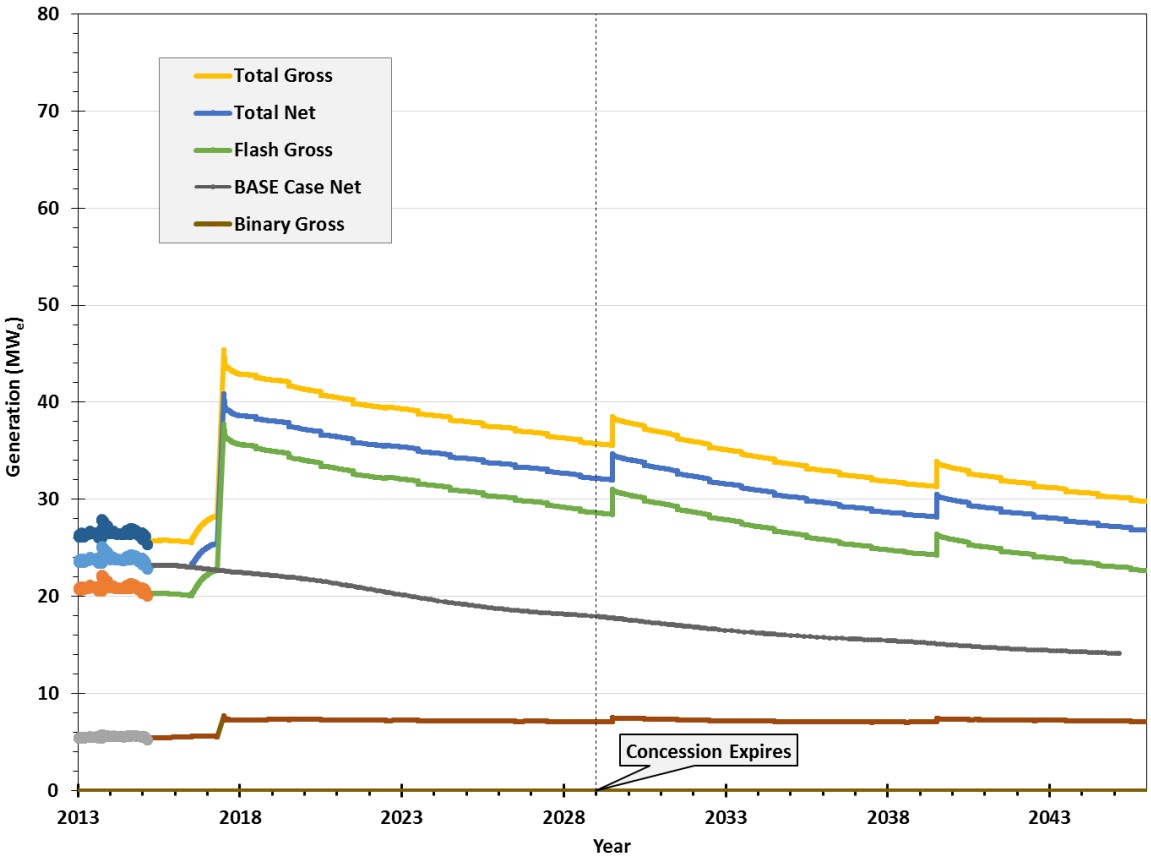

Figure 18. Forecast generation over 30 years with expected results of recommended work plan, including workovers, acidizing, drilling and completion of two new wells in the southern reservoir, but excluding development of the northern area. Annual incremental steps downward are due to reservoir decline and scaling, while larger steps upward reflect workovers.

8.2 Northern Expansion Area

While the northern expansion area at higher elevation on the flank of the volcano, near the primary upwelling, is currently not well defined, a small four-well development was simulated as the minimum development. Modeled responses with this development plan indicate that additional potential production is available in this area, and could be as productive as the southern area. While there is some exploration risk in the in the northern area, which can be substantially mitigated with additional geoscience surveys and study, there is less risk of the wells being affected by thermal breakthrough as has occurred in the southern reservoir.

The forecast, based on the completion of the recommended work and optimization program in the southern area, along with the additional four-well development, shows an increase in net generation from the current output of 22.5 MW_e to 36 MW_e by 2017 (Figure 19). Successful development of the northern area could increase generation to >60 MW_e. This would require refurbishment of Momotombo Unit 2 and additional binary generation capability. Decline, punctuated by the periodic benefit of well workovers every five years, results in generation declining to 51 MW_e by the end of the concession period, and 42 MW_e by the end of the 30-year forecast.

While issues with the second flash unit, additional binary, and lease terms are resolved and further exploration efforts completed, some initial development of the northern area could proceed. This would restore full generation capacity of 42 MW_g to the first flash unit and existing binary unit. One or two new northern wells, with one as a replacement of a southern well, could be drilled initially, followed later by make-up wells to maintain generation at the desired level of 42 MW_g. Development drilling should be initiated on the MT-31 pad, with successive wells moving north along the Bjornsson fault, guided by well drilling and test results. It is apparent that flow is migrating south along the Bjornsson fault from the zone of primary upwelling, and wells could be progressively drilled north along the fault back to the source. The two-well development along the fault would also provide resource confirmation and additional data to proceed with a larger northern development.

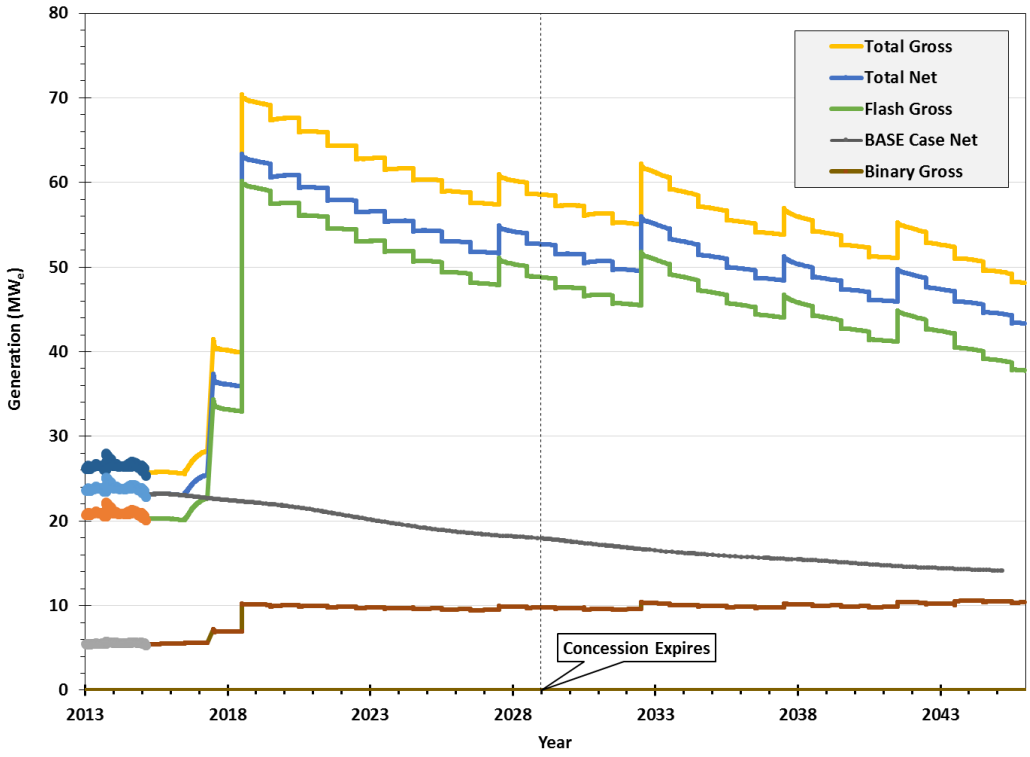

Figure 19. Forecast generation over 30 years with expected results of recommended work plan, including workovers, acidizing, drilling, completion of two new wells in the southern reservoir, and four new wells in the northern undeveloped area. Annual incremental steps downward are due to reservoir decline and scaling, while larger steps upward reflect workovers.

9. CONCLUSIONS

1. Even a 33 year old field can significantly benefit from new geological study and numerical simulation.

2. A numerical model that is constrained to a high degree and coupled with a conceptual model opens new field management possibilities that are not normally associated with numerical modelling.

3. Modelling can detect areas of support in communication with the field that can provide expansion areas for the field.

4. Numerical Simulation can be used to determine the productivity health of wells, and quantify the benefit of possible remediation. It can also detect timing of previous damage to help determine causes of the damage that may be avoided in future wells and operations.

5. Numerical simulation can forecast future production, optimize injection and improve wellfield operations.

6. Simulation can determine the limits that a current field's production area can support as well as potential of expansion areas.

7. Momotombo has four levels which it can raise its generation above its current level:

   a. With just injection optimization and a well repair on OM-54, generation can increase to over 25 MW_e and still be above current levels at the end of the concession period, and above 21 MW_e at the end of the 30 year forecast.

   b. Combine with (a) above, additional remedial well work, and drilling within the existing field, Momotombo can achieve a maximum of 39 MW_e and still be above 32 MW_e at the end of the concession and above 27 MW_e at the end of the forecast period.

   c. Combined with (a) & (b) above, limited expansion up the Bjornsson fault can give Momotombo full output of the existing flash plant and binary plant, increasing generation to 42 MW_e

   d. With additional exploration and added plant infrastructure combined with parts (a), (b) & (c) above, generation can be increased to a minimum of 62 MW_e with construction of new flash and binary production facilities.

10. ACKNOWLEDGMENT

The authors would like to thank Momotombo Power Company for their support in the numerical simulation and conceptual modeling efforts and permission to publish this paper.

11. REFERENCES

Bjornsson, G., 2008. Review of Generating Capacity Estimates for the Momotombo Geothermal Reservoir in Nicaragua. GRC Transactions, Vol. 32.

Geothermal Resource Group, 2016. Numerical Simulation Study, Momotombo Geothermal Field, Nicaragua. Internal Report for Momotombo Power Company, January 2016.

Henley, R.W., and Ellis, A.J. (1983). Geothermal systems ancient and modern: a geochemical review. Earth Science Elsevier, Amsterdam, pp. 1-50.

Martínez, E., Arcia, R., and Sabatino, G., 1988. Geothermal development in Nicaragua. *Geothermics*, 17- 2/3, 333-359.

Moore, J.L., Osbun, E. and Storm, P.V., 1981. Geology and Temperature Distribution of Momotombo Geothermal Field, Nicaragua. AAPG Special Volume SG 12: Energy Resources of the Pacific Region, pp.33-54.

Porras. E.A. and Itoi, R., 2006. The Momotombo Geothermal System and its Conceptual Model. GRC Transactions, vol.30, pp. 33-38.

Porras, E.A., Tanaka, T., Fuji, H., Itoi, R., 2007. Numerical Modeling of the Momotombo geothermal system, Nicaragua, Geothermics Vol. 37.

Porras, E.A., 2009. Geophysical Exploration of the Momotombo Geothermal Field, Nicaragua. Short Course on Surface Exploration for Geothermal Resources, UNU-GTP and LaGeo, El Salvador, 17-30 October, 2009.

Thermochem, 2008. Review of Historical Geochemical Data and Development of a Preliminary Geochemical Conceptual Model for the Momotombo Geothermal Field, Nicaragua. Internal report to Ormat Momotombo Power Company, July 2008.

Trans-Pacific Geothermal Corporation, 2000. Final Report: The Geophysical Exploration of the Momotombo Geothermal Field. Internal Report for Ormat Momotombo Power Company, July 2000.